PROCEEDINGS, 48th Workshop on Geothermal Reservoir Engineering
Stanford University, Stanford, California, February 6-8, 2023
SGP-TR-224

How Precise Can Thermal Breakthrough Predictions Be that Are Derived from Adsorptive Tracer Tests?

Elvar K. Bjarkason

Akita University, Graduate School of International Resource Sciences, 1-1 Tegata-Gakuenmachi, Akita 010-8502, Japan

elvar@mine.akita-u.ac.jp

Keywords: Tracers, adsorbing tracers, injection, temperature decline, uncertainty

ABSTRACT

Tracer tests can provide useful information about the potential impact that injection has on geothermal energy production. Established inert tracer tests are useful for revealing interwell connectivity and providing a quantitative sense of the possible extent of future temperature decline resulting from injection. However, it is understood that conventional inert tracer tests alone do not provide enough information to precisely predict the evolution of temperature decline. Adsorbing tracers can in principle be used to provide precise temperature decline predictions by constraining the effective fluid-rock heat exchange area that controls injection-induced thermal breakthrough. Here we consider how uncertainties in tracer reaction rate parameters affect the precision of thermal breakthrough predictions derived from adsorbing tracer test results.

1. INTRODUCTION

Reinjection of cold, spent production fluid is standard practice and commonly necessary to replenish geothermal reservoirs and ensure that production wells can continue to supply sufficient fluid for commercial energy production operations. This is especially the case for enhanced geothermal systems that rely completely on artificial fluid circulation between wells. Unfortunately, reinjection can reduce energy output from production wells by causing sudden temperature decline (temperature breakthrough). Chemical tracer tests enable early prediction of temperature decline caused by injection. Such predictions can be valuable for optimizing injection strategies and energy extraction. The key properties of tracer tests are that tracer arrival is much earlier than notable temperature breakthrough, and tracer arrival depends on flow parameters that also determine the temperature breakthrough behavior.

Standard inert (non-reactive) tracer tests are useful for estimating the maximum expected temperature change and for bounding the onset of temperature breakthrough. However, injection tests using only a single inert tracer cannot provide information for precise predictions of the time evolution of future temperature decline. This is because an inert tracer alone cannot precisely constrain the flow-path surface area (contact area between the injected fluid and the hot reservoir rock) that determines the rate of temperature decline (see, e.g., (Axelsson et al., 2001; Hawkins et al., 2018, 2020)). Reactive tracers that adsorb to reservoir rock surfaces are a promising tracer technology since adsorptive tracer transport is sensitive to flow-path surface area. Therefore, reactive tracers can in principle be used to constrain flow-path surface areas and provide precise temperature predictions for geothermal applications. However, it has yet to be demonstrated that adsorptive tracer tests can be reliably applied for geothermal field applications. Here we use the terminology "adsorptive tracer test" as a shorthand for a tracer test involving one inert tracer and another adsorbing tracer.

A recent series of tracer and thermal injection experiments (Hawkins et al., 2018, 2020) conducted at a mesoscale experimental well field in Altona, NY, are an important stepping-stone towards demonstrating the applicability of adsorptive tracer tests for geothermal settings. Although the Altona flow experiments were carried out at temperatures below 75°C, the experiments include a thermal breakthrough injection test and an adsorptive tracer test carried out between an injection-production well pair. Those tests are a valuable contribution towards validating the applicability of using reactive tracer tests for thermal breakthrough prediction. Observations from the Altona tests include accurate adsorptive tracer test data and long-term temperature breakthrough data. For those Altona tests, Hawkins et al. (2018) reported a single temperature prediction for a transport model that was calibrated using the adsorptive tracer test. Their predictions were reasonably representative of the observed temperature response; however, their analysis did not include an uncertainty analysis to quantify the reliability of their results. In an important development, Wu et al. (2021) examined the Altona adsorptive tracer data using a finite volume fracture model. They used an ensemble data assimilation framework to calibrate their model and to quantify the model uncertainty. Their modeling results included uncertainty estimates for the temperature predictions. However, their model predictions appeared to show a certain degree of bias toward late thermal breakthrough because their prior parameter distribution biased the prior predictions to late breakthrough. Additionally, they used pressure data along with the adsorptive tracer data to calibrate their model, and they did not fully account for the uncertainty of the adsorptive tracer reaction parameters. Therefore, it does not appear fully clear from their results how reliable adsorptive tracer tests can be expected to be by themselves.

The present study assessed how the estimation precision is fundamentally affected by unavoidable uncertainties in tracer adsorption parameters. In the present study, we examined model-generated tracer test data and assigned prior errors for tracer reaction rate parameters based on measured values reported by Hawkins et al. (2018) for the Altona adsorptive tracer test. Unlike Wu et al. (2021), we used a temperature model and a parameter prior that was not preferentially biased toward late temperature breakthrough. The synthetic tests were unbiased, as the tracer and temperature models used to both generate and analyze the data were the same and therefore perfectly consistent.

Having said that, Wu et al. reported ensemble predictions for two different values of one of the two adsorptive reaction parameters in their model. We, therefore, compared our controlled synthetic results with the predictions reported by Wu et al. (2021). The results in this study complement those found by Wu et al. (2021) as they were found to be consistent. We consider these tests as a helpful benchmark to establish how realistic errors in tracer-rock reaction rate parameters can be expected to affect the precision of temperature breakthrough predictions derived from adsorptive tracer tests.

2. METHODOLOGY

2.1 Modeling Assumptions

2.1.1 Tracer Transport Model

Here we consider a customary conceptual model for tracer transport between an injection well and a production well, where injected tracer flows along a fracture flow channel connecting the two wells. We describe tracer transport along the fracture with a similar model to that used by Hawkins et al. (2018) to account for the flow of both an inert iodide tracer and an adsorbing cesium tracer at the Altona field. Like Wu et al. (2021), we assume that the rock surrounding the fracture is impermeable. Thus, the tracer transport is limited to flow along the fracture and adsorption onto the fracture walls. Ignoring tracer transport within the rock matrix that surrounds the fracture eliminates model variables that can be expected to increase the uncertainty of fracture surface area estimates. Therefore, we consider the present case as a favorable or near-best-case scenario for testing the efficacy of a dual inert-adsorbing tracer test.

For the impermeable rock matrix assumption, the equation presented by Hawkins et al. (2018) for tracer transport within a fracture becomes:

$$\frac{\partial c_f}{\partial t} + v\frac{\partial c_f}{\partial x} - D\frac{\partial^2 c_f}{\partial x^2} = -\frac{A}{V}\frac{\partial \Gamma_f}{\partial t} \quad . \tag{1}$$

The last term in the above equation accounts for the adsorption of the tracer to the fracture (flow-channel) wall. Following Hawkins et al. (2018), we assume that the tracer adsorption is rate-limited and described by

$$\frac{\partial \Gamma_f}{\partial t} = k_{ads}\left(P_f c_f - \Gamma_f\right) \quad . \tag{2}$$

Here t denotes time, c_f is the tracer concentration in the fracture, v is the mean fluid velocity, D is the dispersion coefficient, V is the fracture volume, and Γ_f is the tracer surface concentration on the fracture wall. The distance along the fracture flow direction is given by x. The rate of tracer adsorption to the fracture wall is controlled by the fracture surface area A, the adsorption rate constant k_{ads}, and the adsorption partition coefficient for the fracture wall P_f.

Assuming an instantaneous tracer injection and boundary conditions like those in (Hawkins et al., 2018) gives the following analytical solution in the Laplace domain for the tracer concentration entering the production well from the fracture.

$$\bar{c}_f(s) = \frac{M}{Q_I}\exp\left[\frac{Pe}{2}\left(1-\sqrt{1+\frac{4}{q}\frac{\kappa_f A + sV}{Pe}}\right)\right] = F\frac{M}{q}\exp\left[\frac{Pe}{2}\left(1-\sqrt{1+\frac{4}{q}\frac{\kappa_f A + sV}{Pe}}\right)\right]. \tag{3}$$

Here M is the mass of the injected tracer, Q_I is the volumetric injection rate, and $Pe = vL/D$ defines the Peclet number, where L is the length of the fracture flow-path. The flow rate within the fracture is given by $q = FQ_I$, where F is the fraction of tracer mass recovered at the production well. The tracer adsorption parameters are assigned through (Hawkins et al., 2018)

$$\kappa_f = \frac{sP_f k_{ads}}{k_{ads}+s} \quad . \tag{4}$$

For an adsorbing tracer, we evaluate the tracer concentration at the end of the fracture flow-path $c_f(t, L)$ by inverting the Laplace domain solution in (3). However, for a conservative tracer $\kappa_f = 0$ and the above solution reduces to the following familiar analytical form (see, e.g., (Kreft and Zuber, 1978; Juliusson et al., 2015)):

$$c_f(t, L) = FM\sqrt{\frac{Pe\,V}{4\pi(qt)^3}}\exp\left[-\frac{Pe(V-qt)^2}{4Vqt}\right] \quad . \tag{5}$$

The tracer concentration at the production well c_p is evaluated as $c_p(t) = (q/Q_P)\, c_f(t, L)$ to account for the mixing of the fracture fluid with other produced fluid that is assumed to not contain any tracer when entering the production well.

2.1.2 Thermal Transport Model

For this exercise, we assume that the hydrodynamic dispersion D can be neglected for the thermal transport along the fracture. That is, we apply the commonly used assumption that the thermal transport along the fracture is governed by advection along the flow channel and exchange of heat between the fracture fluid and surrounding reservoir rock through thermal conduction acting perpendicular to the flow direction. Under those conditions, we model the temperature T during injection using the following equations.

$$(\rho C)_w\left(\frac{\partial T_f}{\partial t}+v\frac{\partial T_f}{\partial x}\right)=K_R\frac{A}{V}\frac{\partial T_R}{\partial y}\Big|_{y=\frac{V}{A}} \quad , \quad |y|<\frac{V}{A} \quad . \tag{6}$$

$$(\rho C)_R\frac{\partial T_R}{\partial t}=K_R\frac{\partial^2 T_R}{\partial y^2} \quad , \quad |y|\geq\frac{V}{A} \quad . \tag{7}$$

As before, the subscript f indicates values within the fracture, the subscript R indicates values of the rock surrounding the fracture, and the subscript w labels values of the fluid that fills the fracture channel. The y coordinate indicates the location perpendicular to the fracture plane, and the fracture aperture is given by $2V/A$. Other variables introduced above include the thermal conductivity of the rock K_R, and the density ρ and specific heat capacity C of the rock and fluid.

Solving the above for a homogeneous initial reservoir temperature T_0 and injection starting at $t = 0$ at a constant injection temperature T_I gives

$$T_f(t,L)=T_0-(T_0-T_I)\,\mathrm{erfc}\left[\frac{\eta A}{2q}\left(t-\frac{V}{q}\right)^{-\frac{1}{2}}\right]H\left(t-\frac{V}{q}\right) \quad , \tag{8}$$

where the thermal properties of the rock and fluid have been lumped together in the parameter $\eta=\sqrt{K_R(\rho C)_R}/(\rho C)_w$ (Suzuki et al., 2022). Here $H(\cdot)$ denotes the Heaviside step function. The temperature at the production well is given by

$$T_p(t)=T_0-\frac{FQ_I}{Q_P}\Big(T_0-T_f(t,L)\Big) \quad . \tag{9}$$

This type of temperature model is commonly used in practice along with tracer transport models (see, e.g., (Axelsson et al., 2001; Juliusson et al., 2015)). Here we use this model to quantify the level of precision that can be expected for temperature predictions that are informed by adsorptive tracer tests.

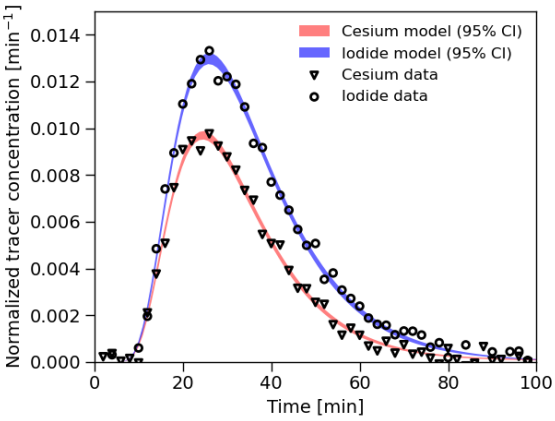

Figure 1: Synthetic tracer concentrations normalized by Q_I/M, where Q_I is the volumetric injection rate and M is the corresponding injected tracer mass. The colored bands show examples of model estimated 95% credible intervals (CIs).

2.2 Reference Model and Observations

In this study, we generated synthetic tracer observations based on a cesium-iodide tracer test carried out at the Altona Field Laboratory (Hawkins et al., 2018). As reported by Hawkins et al., the cesium tracer adsorbs to the reservoir rock while the iodide tracer acts as an inert tracer. For our reference model, we chose tracer reaction parameters based on values reported by Hawkins et al. (2018) for rock samples from the Altona test site. The reference parameters for the flow-channel geometry were chosen to be similar to values reported previously in modeling studies describing observed tracer and thermal breakthrough responses at the Altona field (Hawkins et al., 2018; Suzuki et al., 2022).

In our reference model, we assume that there is one flow channel connecting the injection and production wells. The flow of the injected cesium and iodide tracers, and the temperature breakthrough are assumed to be described by the basic fracture model in Section 2.1. The injection and production rates are equal and set to 5.7 L/min. The initial temperature and injection temperature were set to 11.7°C and 74°C, respectively. The initial pulse of injected tracer solution was considered to contain 200 mg of cesium and 200 mg of iodide. We set the reference Peclet number to 10 and the channel volume to 80 L. Hawkins et al. (2018) analyzed two rock specimens from the Altona site and measured the affinity of cesium to react with the rock samples. They reported measured values of 0.40 and 1.33 d^{-1}, and 7.8 and 16.6 cm for the first-order adsorption rate constant k_{ads} and the partition coefficient P_f, respectively. Here we used the averages of these measured values in the reference model.

For the thermal properties of the fracture fluid and rock, we chose $K_R = 7.6$ W/(m K), $\rho_R = 2{,}500$ kg/m^3, $C_R = 930$ J/(kg K), $\rho_f = 995$ kg/m^3, and $C_f = 4{,}190$ J/(kg K). A recovery ratio of 40% and a 12.6 m^2 fracture surface area were chosen based on the mean posterior estimates of a single fracture model reported in (Suzuki et al., 2022) that matches the observed response for the Altona thermal breakthrough experiment reported by Hawkins et al. (2017, 2018). Using these parameters gave a reference temperature breakthrough profile that is similar to the observed temperature breakthrough curve from the Altona thermal injection test. This allows us to compare the synthetic results reported here with the temperature predictions reported by Wu et al. (2021) for the Altona field. The reference temperature curve is, for instance, shown in Figure 2.

We used the reference tracer transport model to generate cesium and iodide tracer observations. The tracer observations were generated for a tracer injection test lasting 100 minutes and observations were recorded every two minutes. The chosen observation interval is consistent with the early tracer measurements reported by Hawkins et al. (2018). Last, we perturbed the simulated reference tracer concentrations with additive Gaussian noise to serve as observation errors. Like Wu et al. (2021), we chose different absolute values for the noise standard deviations applied to the cesium and iodide data. Although not clearly stated for their Altona tracer analysis, we infer from Wu et al. (2021) that they assumed observation noise standard deviations equal to 3% of the maximum value of each observed tracer curve. Likewise, we assume observation standard deviations equal to 3% of the simulated peak concentrations. With this choice, the observation noise standard deviations were about 0.013 and 0.01 ppm for the iodide and cesium data, respectively.

Figure 1 shows the resulting tracer observations normalized by multiplying the concentrations with the injection rate Q_I and dividing by the corresponding injected tracer mass M. Discounting for the fact that the present study does not include tracer recirculation unlike the actual Altona field test, the tracer curves in Figure 1 look more dispersed than those reported in (Hawkins et al., 2018). This difference is, firstly, because the calibrated model used by Hawkins et al. (2018) treats the mixing of the injected fluid and the production fluid in a different way to the present model. Secondly, the model parameters used are different. Nevertheless, we think that the synthetic reference tracer and temperature profiles, and the Altona field observations analyzed by Wu et al. (2021) are similar enough for our purposes.

Table 1: Prior parameter assumptions and posterior estimated parameter statistics for the baseline test case. Here σ denotes the parameter standard deviation. For the posterior parameter estimates, we also report the estimated 95% credible interval (CI) centered around the posterior mean.

Parameter	Prior		Posterior estimates		
	Mean	σ	Mean	σ	95% CI
$\log_{10}(A)$	1.10	2.00	1.1	0.1	[0.9, 1.4]
$\log_{10}(k_{ads})$	-5.00	0.13	-5.1	0.1	[-5.3, -4.8]
$\log_{10}(P_f)$	-0.91	0.08	-0.92	0.08	[-1.07, -0.75]

Table 2: Prior parameter assumptions and posterior estimated parameter statistics for a case with six unknown parameters. Here σ denotes the parameter standard deviation. For the posterior parameter estimates, we also report the estimated 95% credible interval (CI) centered around the posterior mean.

Parameter	Prior		Posterior estimates		
	Mean	σ	Mean	σ	95% CI
$\log_{10}(A)$	1.10	2.00	1.2	0.1	[0.9, 1.4]
$\log_{10}(k_{ads})$	-5.00	0.13	-5.1	0.1	[-5.3, -4.8]
$\log_{10}(P_f)$	-0.91	0.08	-0.91	0.08	[-1.08, -0.75]
$\log_{10}(V)$	-1.10	1.00	-1.089	0.006	[-1.102, -1.076]
$\log_{10}(Pe)$	1.00	1.00	0.996	0.008	[0.980, 1.012]
F	0.40	0.10	0.408	0.004	[0.400, 0.417]

2.3 Accounting for Model Uncertainty

We apply Bayesian principles to elucidate expected uncertainties associated with estimating thermal breakthrough based on the above synthetic adsorbing tracer test. More specifically, we use an approximate Bayesian sampler called the randomized maximum likelihood (RML) method (Oliver et al., 1996; Oliver, 2017) to quantify how precise we can expect to estimate thermal breakthrough model parameters and the associated future temperature changes during production from geothermal fields. Notably, we focus on estimating the fracture surface area, which mainly controls the thermal breakthrough trend, and we consider how realistic errors for the adsorption reaction parameters impact the estimation precision.

The implemented RML estimation procedure requires the tracer observations, a Gaussian observation noise model (here we assume the same noise model that was used to generate the synthetic observations), and a way of accessing model-generated tracer concentrations for given model parameters. Here we used the same basic RML implementation that was used successfully by Suzuki et al. (2022) to estimate flow-path surface areas based on thermal breakthrough data. The RML method outputs an ensemble of N_e models that are generated through a stochastic optimization process, which involves matching the chosen tracer model with randomly generated observation samples. Here we chose to use $N_e = 1{,}000$. The resulting ensemble can be used to estimate the so-called posterior model parameter uncertainty given the data and model assumptions. In addition, the RML method requires inputting a Gaussian prior distribution for the model parameters to quantify prior knowledge about the plausible ranges for the parameter values. Here we assumed that the prior uncertainty of individual model parameters is described fully by a prior mean and a prior standard deviation.

Here we considered two main test cases to showcase what adsorbing tracer tests might be expected to reveal about future injection-induced temperature changes. First, we looked at an ideal case where the surface area is the only unknown. Second, we considered a baseline case with the surface area and the adsorption parameters k_{ads} and P_f as the unknowns. All other parameters were assumed to be known. In both cases, we log-transformed the adjustable parameters for the estimation, and we always used the same prior statistics for the log-transformed surface area. Table 1 outlines the prior assumptions made for the baseline case. Notice that for this exercise we used a perfect and unbiased parameter prior mean that corresponds with the true reference parameter values. This is because we simply wanted to focus on how parameter uncertainties affect the precision of the temperature predictions, and we were not interested in exploring how reliable the estimates might be for imperfect prior assumptions.

Perhaps a bit optimistically, we assumed for the baseline case that most of the models sampled from the prior have cesium adsorption parameters k_{ads} and P_f that fall within the ranges of the measured values reported by Hawkins et al. (2018). The prior 95% credible interval (CI) indicates that k_{ads} mainly ranges from about 0.5 to 1.6 d^{-1}, and P_f mainly ranges from about 8.4 to 17.8 cm. However, since those ranges are only approximately (and optimistically) informed by two measurements, we also considered a more pessimistic case where the prior standard deviations for the log-transformed adsorption parameters are twice as large. In that case, the prior 95% credible interval (CI) indicates that k_{ads} mainly ranges from about 0.3 to 2.9 d^{-1}, and P_f mainly ranges from about 5.7 to 26.0 cm.

We also considered a case with a total of six unknowns, which also includes the recovery ratio, and the log-transformed values of the fracture volume and the Peclet number (see Table 2). The assumed prior standard deviations for the six-parameter case are provided in Table 2. For all test cases, we chose the same wide prior distribution for $\log_{10}(A)$ by setting its prior standard deviation to 2.

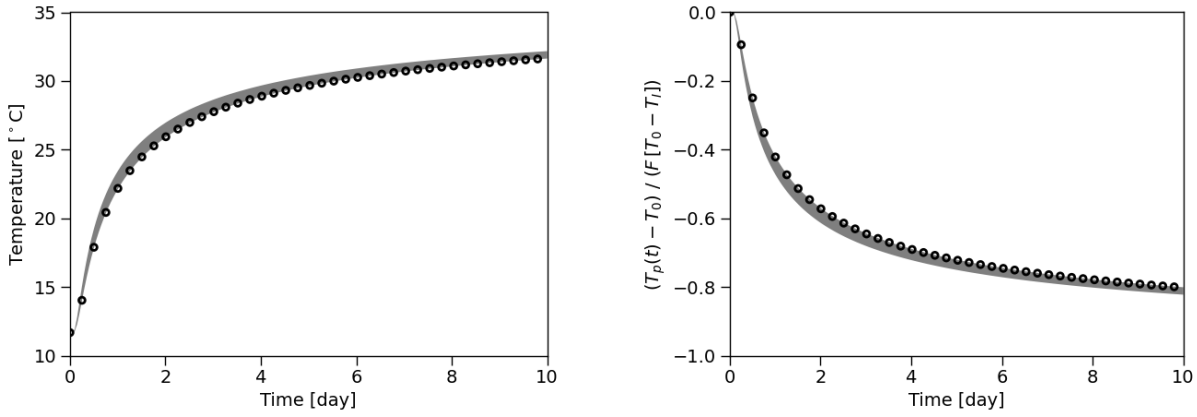

Figure 2: Estimated (Left) temperature breakthrough curve and (Right) normalized temperature change. The results shown are for an ideal case where the surface area is the only unknown. The gray intervals indicate the estimated 95% CIs, and the reference temperature curve is shown for comparison using the black circles.

3. RESULTS

3.1 Known Adsorption Parameters

First, we consider the case of known reaction parameters and assume that the surface area is the only uncertain parameter. In this case, we only matched the synthetic cesium data since the inert iodide response curve is uniquely defined. After running the RML algorithm to estimate the surface area, the resulting match to the cesium data looks similar to that shown in Figure 4. As we might expect, the value of $\log_{10}(A)$ was estimated precisely; the estimated posterior mean, standard deviation, and 95% CI were respectively 1.08, 0.01, and [1.05, 1.10]. As a result, the range for the future temperature changes was estimated precisely but with the true reference temperature response lying on the edge of the estimated 95% CI, as shown in Figure 2. Following Wu et al. (2021), we show the temperature breakthrough curve for the first ten days of injection.

Figure 2 also depicts a normalized temperature curve given by $T_N(t) = \big(T_p(t) - T_0\big)/(F[(T_0 - T_I)])$. The normalized temperature curve is useful for visualizing how large the estimated temperature change is relative to the maximum possible reference temperature change: $T_N(t) = 0$ coincides with zero temperature change, and $T_N(t) = -1$ for the maximum temperature change (for the given reference

recovery ratio F). As shown, the reference temperature response reaches about 80% of its maximum attainable temperature change after ten days of injection.

In addition to estimating the surface area, we considered the uncertainties of other parameters affecting the tracer recovery. Namely, we also looked at the effect of uncertain volume, Peclet number, and recovery ratio parameters. For this example, the adsorption parameters are again assumed to be perfectly known, while the prior assumptions for the other parameters were the same as those listed in Table 2. For this case, we estimated the transport parameters based on the iodide and cesium data, since the main parameters controlling the inert iodide response are now unknown and the inert iodide response is needed as a reference to gauge how strongly the cesium is adsorbed. The resulting temperature predictions are shown in Figure 3. The additional unknown parameters governing the inert tracer transport had little impact on the precision of the temperature predictions for this example and the level of observation noise. The 95% CIs for the normalized temperature profiles indicate that the temperature estimation error is within 10% of the maximum temperature change for the examples in Figures 2 and 3. These examples serve to illustrate that adsorbing tracers can in principle be used to provide highly accurate and precise temperature predictions assuming that the tracer adsorption parameters are well known and that the tracer transport model is appropriately chosen.

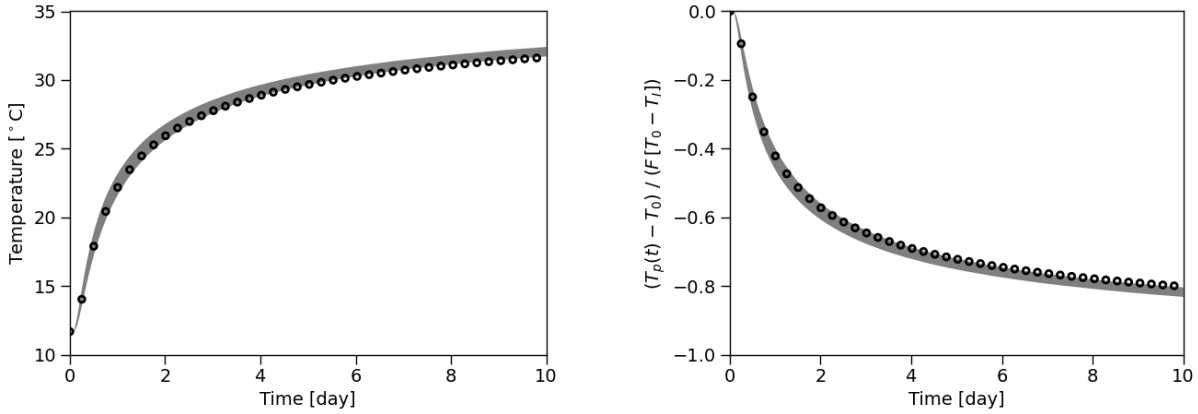

Figure 3: Estimated (Left) temperature breakthrough curve and (Right) normalized temperature change. The results shown are for a case where the cesium tracer adsorption parameters are known but the other tracer transport parameters listed in Table 2 are uncertain. The gray intervals indicate the estimated 95% CIs, and the reference temperature curve is shown for comparison using the black circles. For the normalization, we used the true reference recovery ratio F.

3.2 Uncertain Adsorption Parameters

Next, we considered the impact of realistic cesium adsorption parameter uncertainties. As mentioned previously, the prior uncertainties of the adsorption parameters were based on measured values reported by Hawkins et al. (2018). First, we considered the baseline case for which the prior parameter assumptions are given in Table 1. The baseline example only involved estimating the unknown surface area and two additional parameters governing the cesium adsorption. Therefore, we only carried out the baseline estimation by analyzing the cesium data.

Figure 4 shows the matched cesium tracer profile for the baseline case. The estimated posterior parameter statistics are provided in Table 1. The surface area appears to have been estimated accurately. The 95% CI suggested that the surface area is likely to range between about 7 and 25 m^2, which is consistent with the 12.6 m^2 reference surface area. The adsorption partition coefficient P_f was not sensitive to the observations and its posterior distribution did not markedly change from the prior. The adsorption rate constant k_{ads} was found to be slightly sensitive to the present setup and observations, which resulted in its posterior mean being slightly lower than the reference value.

The estimated future temperature range predicted for the baseline case is shown in Figure 5. The results show that the temperature predictions are quite sensitive to realistic errors for the adsorption reaction parameters. For the baseline case shown in Figure 5, the maximum width of the temperature 95% CI is about 13°C. The corresponding width for the normalized temperature change is 53% of the maximum possible change. After about six days of injection, the 95% CI indicates that we can expect the temperature to be between 24.5 and 32.9°C, which is a range of 8.4°C. The test for the six-parameter case gave results that were comparable to the baseline case (see Table 2 and Figure 6). Therefore, we draw the same conclusion as in Section 3.1 that uncertainties for the adsorption rate and partition parameters dominate the temperature prediction precision for the present setup.

Wu et al. (2021) applied an ensemble-based data assimilation framework to predict the thermal breakthrough observed during the thermal injection field test at the Altona test site. They used cesium-iodide tracer test data to estimate a heterogeneous fracture aperture distribution in their finite volume fracture model. Additionally, they used pressure loss data to inform their estimation. Wu et al. considered matching the cesium tracer response data using two values of 7.8 and 15.0 cm for the partition coefficient P_f. Their resulting temperature estimates were shown to coincide well with the observed field response, and their estimates ranged from about 21.7 to 31.5°C after six days of injection. Their temperature range after six days is slightly wider but fairly consistent with our synthetic results (9.8°C instead of 8.4°C). These results indicate that the additional pressure data used by Wu et al. may have had little impact on their estimates. It would, therefore,

be interesting to consider the significance of using additional pressure loss data along with the adsorptive tracer data. Furthermore, the Altona field analysis results from (Wu et al., 2021) and the synthetic results presented here suggest that uncertainties associated with reaction rates of adsorbing tracers can be expected to dominate the precision level of thermal breakthrough predictions that are estimated based on adsorbing tracer tests.

From the limited number of rock samples analyzed by Hawkins et al. (2018), it is unclear what is a reasonable prior range for the cesium adsorption parameters. The prior assumptions for the baseline case might be rather optimistic. For that reason, we also considered a more conservative setup where we doubled the baseline prior standard deviations for the log-transformed adsorption rate and partition parameters. Otherwise, the other prior assumptions were the same as before for the baseline case. Figure 5 shows the resulting predicted temperature intervals in red. The maximum temperature range shown for the 95% CI, in this case, is almost 20°C. This corresponds to about 80% of the maximum temperature change, and the estimated normalized temperature range was not narrowed down by much more than the maximum possible range of temperature values for the considered ten-day injection period. This illustrates that the value of adsorbing tracer tests could be limited if the relevant tracer adsorption parameters can be expected to vary over a wide range in geothermal fields. These results indicate that this type of tracer test is unlikely to result in as accurate temperature predictions as might be anticipated, for example, based on ideal test conditions reflect by the cases in Figures 2 and 3. These conclusions are consistent with the field application results reported by Wu et al. (2021).

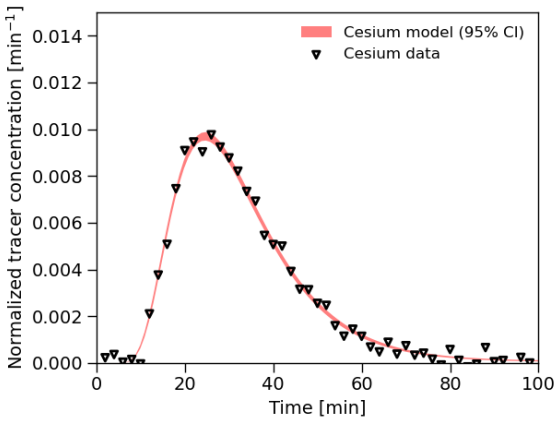

Figure 4: Synthetic adsorbing cesium tracer concentrations normalized by Q_I/M, where Q_I is the volumetric injection rate and M is the injected mass of cesium. The colored band shows the model estimated 95% credible intervals (CIs) for the baseline test case outlined in Table 1.

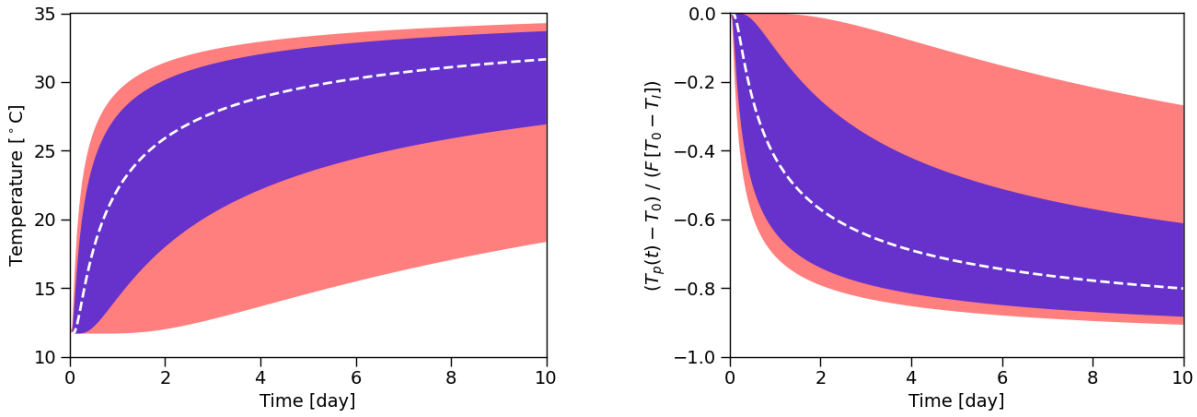

Figure 5: Estimated (Left) temperature breakthrough curve and (Right) normalized temperature change. The colored intervals indicate the estimated 95% CIs, and the reference temperature curve is illustrated by the white dashed curve. (Blue interval) Results for the baseline case outlined in Table 1. (Red interval) Results after doubling the prior standard deviation for the two log-transformed adsorption parameters.

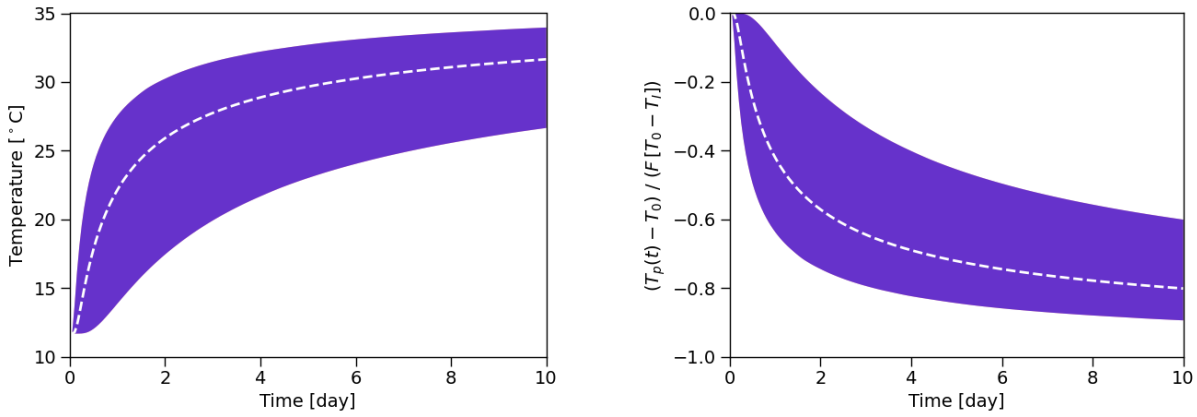

Figure 6: Estimated (Left) temperature breakthrough curve and (Right) normalized temperature change. The colored intervals indicate the estimated 95% CIs for the six-parameter test case outlined in Table 2, and the reference temperature curve is illustrated by the white dashed curve. For the normalization, we used the true reference recovery ratio *F*.

4. CONCLUSION

This study looked at the reliability of thermal breakthrough predictions that are made based on transport models calibrated using data from adsorptive tracer tests. The analysis was based on synthetic tracer test models that were fabricated to be consistent with recent thermal and tracer injection tests carried out at a mesoscale experimental well field in Altona, NY. The results indicate that nearly ideal adsorptive tracer tests with known adsorption parameters and observation errors on the order of 3% of the peak tracer concentrations can result in predictions for injection-induced temperature changes with prediction errors of less than 10%. However, that ideal scenario is unrealistic for field applications, and we should expect larger prediction errors when considering realistic uncertainties for tracer reaction rate parameters.

In light of previously reported measured ranges for reaction parameters used to describe cesium adsorption onto rock samples collected from the Altona site, we looked at two plausible scenarios for the level of uncertainty for the adsorption parameters: one optimistic baseline case and another more pessimistic case. For the baseline case, the uncertainty of the predicted temperature range was on the order of 30–50% of the maximum temperature change. The same uncertainty measure was considerably larger for the pessimistic case or about 60–80% of the maximum temperature change. The baseline test results were shown to be consistent with uncertainty quantification results reported by Wu et al. (2021) for an adsorptive tracer test carried out at Altona. Therefore, the presented synthetic test cases appear to provide a reasonable benchmark of what can be learned from adsorptive tracer tests. Lastly, we concluded that uncertainties related to the parameters describing the tracer adsorption kinetics can be expected to dominate thermal breakthrough prediction errors for practical adsorptive tracer tests with small observation errors.

REFERENCES

Axelsson, G., Flovenz, O.G., Hauksdottir, S., Hjartarson, A., & Liu, J. (2001). Analysis of tracer test data, and injection-induced cooling, in the Laugaland geothermal field, N-Iceland. *Geothermics*, 30(6), 697–725.

Hawkins, A.J., Becker, M.W., & Tester, J.W. (2018). Inert and adsorptive tracer tests for field measurement of flow-wetted surface area. *Water Resources Research*, 54(8), 5341–5358.

Hawkins, A.J., Fox, D.B., Becker, M.W., & Tester, J.W. (2017). Measurement and simulation of heat exchange in fractured bedrock using inert and thermally degrading tracers, *Water Resources Research*, 53(2), 1210–1230.

Hawkins, A.J., Fox, D.B., Koch, D.L., Becker, M.W., & Tester, J.W. (2020). Predictive inverse model for advective heat transfer in a short-circuited fracture: Dimensional analysis, machine learning, and field demonstration. *Water Resources Research*, 56(11), e2020WR027065.

Juliusson, E., Markusson, S., & Sigurdardottir, A. (2015). Phase-specific and phase-partitioning tracer experiment in the Krafla reservoir, Iceland. *Proceedings, World Geothermal Congress 2015*. Melbourne, Australia.

Kreft, A., & Zuber, A. (1978). On the physical meaning of the dispersion equation and its solutions for different initial and boundary conditions. *Chemical Engineering Science*, 33(11), 1471–1480.

Oliver, D.S. (2017). Metropolized randomized maximum likelihood for improved sampling from multimodal distributions. *SIAM/ASA Journal on Uncertainty Quantification,* 5(1), 259–277.

Oliver, D.S., He, N., & Reynolds, A.C. (1996). Conditioning permeability fields to pressure data. *Proceedings of the 5th European Conference on the Mathematics of Oil Recovery*. Leoben, Austria, pp. 259–270.

Suzuki, A., Bjarkason, E.K., Yamaguchi, A., Hawkins, A.J., & Hashida, T. (2022). Estimation of flow-channel structures with uncertainty quantification: Validation by 3D-printed fractures and field application. *Geothermics*, 105, 102480.

Wu, H., Fu, P., Hawkins, A.J., Tang, H., & Morris, J.P. (2021). Predicting thermal performance of an enhanced geothermal system from tracer tests in a data assimilation framework. *Water Resources Research*, 57(12), e2021WR030987.